Structural Diversity in Iron(II) Complexes of 2,6-Di(pyrazol-1-yl)pyridine and 2,6-Di(3-methylpyrazol-1-yl)pyridine

Jérôme Elhaïk, Colin A. Kilner and Malcolm A. Halcrow*.

School of Chemistry, University of Leeds, Woodhouse Lane, Leeds, U.K. LS2 9JT.
Email: M.A.Halcrow@chem.leeds.ac.uk

Supplementary Information

Synthesis and crystal structure determinations of $[Fe(L^2)_2][BF_4]_2{\cdot}4CH_3CN$

Table S1 Experimental details for the single crystal structures of $[Fe(L^2)_2][BF_4]_2{\cdot}4CH_3CN$

Synthesis and crystal structure determinations of $[Fe(L^2)_2][ClO_4]_2{\cdot}(CH_3)_2CO$

Table S2 Experimental details for the single crystal structures of $[Fe(L^2)_2][ClO_4]_2{\cdot}(CH_3)_2CO$

Fig. S1 View of the complex dication in the crystal structure of $[Fe(L^2)_2][BF_4]_2{\cdot}4CH_3CN$ at 250 K, showing the atom numbering scheme employed.

Table S3 Selected bond lengths and angles (Å, °) for $[Fe(L^2)_2][BF_4]_2{\cdot}4CH_3CN$.

Table S4 Selected bond lengths and angles (Å, °) for $[Fe(L^2)_2][ClO_4]_2{\cdot}(CH_3)_2CO$.

Table S5 Selected structural parameters (Å, °) for $[Fe(L^2)_2][BF_4]_2{\cdot}4CH_3CN$ and $[Fe(L^2)_2][ClO_4]_2{\cdot}(CH_3)_2CO$, used to monitor their spin states at different temperatures.

Fig. S2 Plot of the variation of the Fe–N bond lengths with temperature in $[Fe(L^2)_2][BF_4]_2{\cdot}4CH_3CN$ and $[Fe(L^2)_2][ClO_4]_2{\cdot}(CH_3)_2CO$.

Table S6 C–H...I hydrogen bond distances and angles (Å, °) in $[Fe(L^1)_2]I_{0.5}[I_3]_{1.5}$ (**1**).

Synthesis and crystal structure determinations of $[Fe(L^2)_2][BF_4]_2{\cdot}4CH_3CN$

Iron(II) tetrafluoroborate hexahydrate (0.11 g, 3.1 x 10^{-4} mol) and 2,6-di(3-methylpyrazol-1-yl)pyridine (0.15 g, 6.3 x 10^{-4} mol) were stirred in acetonitrile (50 cm^3) at room temperature until all the solid had dissolved. The resultant yellow solution was concentrated to 5 cm^3 and filtered. Slow diffusion of diethyl ether vapour into this solution yielded mustard yellow crystals, which decomposed to a solvent-free powder upon drying. Yield 0.19 g, 86 %. Found: C, 44.1; H, 3.9; N, 19.8 %. Calcd. for $C_{26}H_{26}B_2F_8FeN_{10}$: C, 44.1; H, 3.7; N, 19.8 %. Electrospray mass spectrum m/z = 267 $[^{56}FeL_2]^{2+}$, 240 $[L+H]^+$.

Experimental details for the structure determinations of $[Fe(L^2)_2][BF_4]_2{\cdot}4CH_3CN$ are given in Table S1. Their air-sensitivity meant that the crystals used decomposed between measurements. Hence, while the same crystal was used for the structure determinations at 100 and 200 K, two different crystals were required for the 150 and 250 K measurements. These latter two crystals, at 150 and 250 K, were of the opposite hand to the crystal used at 100 and 200 K. An attempted data collection at 300 K failed because the crystal decomposed. One of the two BF_4^- anions, B(43)-F(47), is disordered at all four temperatures. At 200 and 250 K this was modelled over three sites labelled 'A' (occupancy 0.4), 'B' (occupancy 0.4) and 'C' (occupancy 0.2). At 100 and 150 K only two disorder sites for this ion were located, which were labelled 'A' (occupancy 0.6) 'B' (occupancy 0.4). These were modelled using the refined restraints B–F = 1.38(2) and 1,3-F...F = 2.25(2) Å at 150 K, and B–F = 1.39(2) and 1,3-F...F = 2.27(2) Å at all the other temperatures. At all temperatures, all non-H atoms with occupancy > 0.5 were refined anisotropically. All H atoms were placed in calculated positions and refined using a riding model, with the methyl group torsions allowed to refine freely.

Table S1 Experimental details for the single crystal structures of $[Fe(L^2)_2][BF_4]_2{\cdot}4CH_3CN$ ($C_{34}H_{38}B_2F_8FeN_{14}$, M_r 872.25, orthorhombic, space group $P2_12_12_1$, $Z = 4$).

T(K)	100(2)	150(2)	200(2)	250(2)
a (Å)	11.2572(1)	11.3871(1)	11.5476(1)	11.6508(1)
b (Å)	13.5578(1)	13.6181(1)	13.6803(1)	13.7476(1)
c (Å)	26.1701(2)	26.2355(3)	26.3236(2)	26.4113(3)
V (Å^3)	3994.16(6)	4068.36(7)	4158.46(6)	4230.31(7)
μ (Mo-K$_\alpha$) (mm^{-1})	0.461	0.453	0.443	0.435
Measured reflections	65112	67255	80961	70076
Independent reflections	9152	9331	9499	9695
R_{int}	0.078	0.072	0.052	0.091
$R(F)$[a]	0.034	0.041	0.037	0.042
w$R(F^2)$[b]	0.089	0.107	0.105	0.123
Goodness of fit	1.033	1.026	1.025	1.047
Flack parameter	–0.025(11)	–0.017(14)	–0.013(12)	–0.014(15)

[a] $R = \Sigma[\,|F_o| - |F_c|\,] / \Sigma|F_o|$ [b] $wR = [\Sigma w(F_o^2 - F_c^2) \;/\; \Sigma wF_o^4]^{½}$

Synthesis and crystal structure determinations of $[Fe(L^2)_2][ClO_4]_2{\cdot}(CH_3)_2CO$

A mixture of iron(II) perchlorate hexahydrate (0.11 g, 3.1 x 10^{-4} mol) and 2,6-di(3-methylpyrazol-1-yl)pyridine (0.15 g, 6.3 x 10^{-4} mol) in acetone (50 cm^3) was stirred at room temperature for 30 mins. This gave a yellow solution, that was concentrated to 5 cm^3 and filtered. Slow diffusion of diethyl ether vapour into this solution yielded mustard yellow crystals, which decomposed to a solvent-free powder upon drying. Yield 0.15 g, 64 %. Found: C, 42.6; H, 3.6; N, 19.3 %. Calcd. for $C_{26}H_{26}Cl_2FeN_{10}O_8$: C, 42.6; H, 3.6; N, 19.1 %. Electrospray mass spectrum m/z = 267 $[^{56}FeL_2]^{2+}$, 240 $[L+H]^+$. **CAUTION** although we have experienced no difficulties when handling this compound, metal-organic perchlorates are potentially explosive and should be handled with due care in small quantities.

Experimental details for the structure determinations of $[Fe(L^2)_2][ClO_4]_2{\cdot}(CH_3)_2CO$ are given in Table S2. Their air-sensitivity meant that the crystals used decomposed between measurements. For that reason, different crystals were used for all four structure determinations. An attempted data collection at 300 K failed because the crystal decomposed. At all the temperatures examined, both ClO_4^- anions and the acetone solvent molecule are disordered. The disordered model used for the anions was the same at all four temperatures. Anion Cl(38)-O(42) was modelled in all four structures over two equally occupied sites, labelled 'A' and 'B', while ion Cl(43)-O(47) was modelled using three partial anion sites labelled 'A' (occupancy 0.35), 'B' (occupancy 0.35) and 'C' (occupancy 0.30). The following restraints were applied to both anions: Cl–O = 1.43(2) and 1,3-O...O = 2.34(2) Å at 250 K; Cl–O = 1.44(2) and 1,3-O...O = 2.35(2) Å at 150 and 200 K; and Cl–O = 1.45(2) and 1,3-O...O = 2.37(2) Å at 100 K. The acetone molecule C(48)-O(51) was disordered over two equally occupied sites 'A' and 'B' at 200 and 250 K, while three distinct sites were resolvaed at lower temperatures, labelled 'A', 'B' and 'C'. These were refined with relative occupancies 0.40:0.40:0.20 at 150 K, and 0.45:0.45:0.10 at 100 K. The following refined restraints were applied to this molecule: at 250 K, C–C = 1.49(2), C=O = 1.24(2) and 1,3-C...O = 2.36(2) Å; at 200 K, C–C = 1.48(2), C=O = 1.25(2) and 1,3-C...O = 2.38(2) Å; at 150 K, C–C = 1.49(2), C=O = 1.23(2) and 1,3-C...O = 2.39(2) Å; and at 100 K, C–C = 1.49(2), C=O = 1.26(2) and 1,3-C...O = 2.40(2) Å. At all temperatures, all crystallographically ordered non-H atoms were refined anisotropically, while all H atoms were placed in calculated positions and refined using a riding model, with the methyl group torsions allowed to refine freely.

Table S2 Experimental details for the single crystal structures of $[Fe(L^2)_2][ClO_4]_2{\cdot}(CH_3)_2CO$ ($C_{29}H_{32}Cl_2FeN_{10}O_9$, M_r 791.40, monoclinic, space group $C2/c$, $Z = 8$).

T (K)	100(2)	150(2)	200(2)	250(2)
a (Å)	22.7743(3)	22.8777(2)	23.1702(4)	23.3113(3)
b (Å)	10.9586(2)	11.0240(1)	11.1910(2)	11.2528(2)
c (Å)	28.4036(4)	28.3914(3)	28.3275(5)	28.4066(4)
β (°)	106.1525(9)	106.3318(7)	107.0868(9)	107.3076(8)
V (Å^3)	6809.00(18)	6871.48(11)	7021.0(2)	7114.13(19)
μ (Mo-K$_\alpha$) (mm^{-1})	0.668	0.662	0.648	0.640
Measured reflections	51437	48139	27294	35705
Independent reflections	7823	7909	7625	8106
R_{int}	0.123	0.090	0.080	0.183
$R(F)$[a]	0.054	0.062	0.068	0.085
w$R(F^2)$[b]	0.165	0.196	0.205	0.256
Goodness of fit	1.042	1.109	1.045	1.042

[a] $R = \Sigma[\,|F_o| - |F_c|\,] / \Sigma|F_o|$ [b] $wR = [\Sigma w(F_o^2 - F_c^2) \;/\; \Sigma wF_o^4]^{½}$

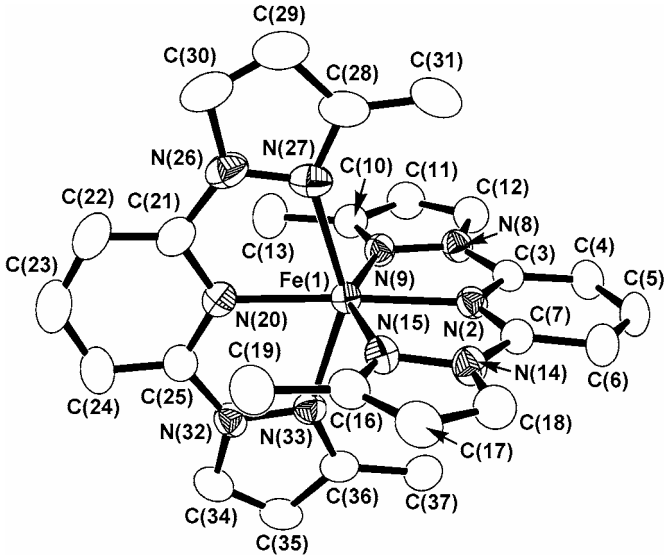

Fig. S1 View of the complex dication in the crystal structure of $[Fe(L^2)_2][BF_4]_2 \cdot 4CH_3CN$ at 250 K, showing the atom numbering scheme employed. All H atoms have been omitted, and thermal ellipsoids are at the 35 % probability level. The complex dication in $[Fe(L^2)_2][ClO_4]_2 \cdot (CH_3)_2CO$ is visually almost identical to the one here, and uses the same atom numbering scheme.

Table S3 Selected bond lengths and angles (Å, °) for $[Fe(L^2)_2][BF_4]_2 \cdot 4CH_3CN$. The angles '$\phi$' and '$\theta$' are defined in Scheme 1.

T (K)	100	150	200	250
Fe(1)–N(2)	1.9107(16)	1.9696(19)	2.0627(16)	2.102(2)
Fe(1)–N(9)	2.0090(17)	2.047(2)	2.1220(17)	2.155(2)
Fe(1)–N(15)	2.0134(17)	2.066(2)	2.1501(17)	2.184(2)
Fe(1)–N(20)	1.9084(17)	1.957(2)	2.076(2)	2.112(2)
Fe(1)–N(27)	1.9982(16)	2.026(2)	2.129(2)	2.160(2)
Fe(1)–N(33)	2.0055(17)	2.051(2)	2.1401(18)	2.177(2)
N(2)–Fe(1)–N(9)	79.45(7)	77.88(8)	75.58(6)	74.69(8)
N(2)–Fe(1)–N(15)	79.82(7)	78.02(8)	75.37(6)	74.37(8)
N(2)–Fe(1)–N(20) (ϕ)	177.20(7)	177.13(9)	176.48(7)	176.52(8)
N(2)–Fe(1)–N(27)	100.58(7)	102.04(10)	106.57(8)	107.49(9)
N(2)–Fe(1)–N(33)	99.97(7)	101.27(9)	103.78(7)	104.57(8)
N(9)–Fe(1)–N(15)	159.27(7)	155.90(8)	150.95(6)	149.06(8)
N(9)–Fe(1)–N(20)	103.29(7)	104.85(8)	107.61(7)	108.39(8)
N(9)–Fe(1)–N(27)	91.05(7)	91.68(9)	93.46(7)	94.23(9)
N(9)–Fe(1)–N(33)	91.52(7)	92.09(8)	93.28(7)	93.67(8)
N(15)–Fe(1)–N(20)	97.44(7)	99.26(8)	101.44(7)	102.55(8)
N(15)–Fe(1)–N(27)	92.48(7)	93.04(9)	94.40(7)	94.81(9)
N(15)–Fe(1)–N(33)	92.31(7)	92.86(8)	93.93(6)	94.19(8)
N(20)–Fe(1)–N(27)	80.04(7)	78.90(11)	74.97(9)	74.18(10)
N(20)–Fe(1)–N(33)	79.50(7)	77.87(9)	74.78(7)	73.83(8)
N(27)–Fe(1)–N(33)	159.42(7)	156.66(10)	149.64(9)	147.94(9)
θ	89.65(2)	89.69(2)	89.40(2)	89.53(3)

Table S4 Selected bond lengths and angles (Å, °) for $[Fe(L^2)_2][ClO_4]_2\cdot(CH_3)_2CO$. The angles 'ϕ' and 'θ' are defined in Scheme 1.

T (K)	100	150	200	250
Fe(1)–N(2)	1.900(2)	1.933(3)	2.087(3)	2.112(3)
Fe(1)–N(9)	1.989(2)	2.016(3)	2.156(3)	2.182(3)
Fe(1)–N(15)	2.006(2)	2.026(3)	2.150(3)	2.170(3)
Fe(1)–N(20)	1.905(2)	1.945(3)	2.086(3)	2.117(3)
Fe(1)–N(27)	2.007(2)	2.029(3)	2.139(3)	2.161(3)
Fe(1)–N(33)	2.002(2)	2.036(3)	2.170(3)	2.204(3)
N(2)–Fe(1)–N(9)	80.00(9)	79.25(12)	74.40(11)	73.51(12)
N(2)–Fe(1)–N(15)	79.86(9)	79.07(12)	74.65(11)	74.24(12)
N(2)–Fe(1)–N(20) (ϕ)	177.98(10)	178.08(12)	176.29(10)	176.10(12)
N(2)–Fe(1)–N(27)	99.80(9)	101.71(11)	108.86(11)	110.10(12)
N(2)–Fe(1)–N(33)	100.71(9)	100.94(11)	102.19(10)	102.45(12)
N(9)–Fe(1)–N(15)	159.76(10)	158.19(13)	148.93(12)	147.65(14)
N(9)–Fe(1)–N(20)	101.96(10)	102.60(12)	107.10(12)	107.86(13)
N(9)–Fe(1)–N(27)	90.58(9)	90.73(11)	91.00(11)	91.18(12)
N(9)–Fe(1)–N(33)	91.08(9)	91.01(11)	92.33(11)	92.99(13)
N(15)–Fe(1)–N(20)	98.21(10)	99.06(12)	103.64(11)	104.16(13)
N(15)–Fe(1)–N(27)	94.69(9)	95.91(11)	101.42(11)	102.24(13)
N(15)–Fe(1)–N(33)	90.79(9)	90.83(11)	91.58(11)	91.39(13)
N(20)–Fe(1)–N(27)	79.75(10)	78.84(11)	74.63(11)	73.65(13)
N(20)–Fe(1)–N(33)	79.82(9)	78.61(11)	74.47(10)	73.94(12)
N(27)–Fe(1)–N(33)	159.40(9)	157.21(11)	148.51(11)	147.02(13)
θ	87.45(3)	86.88(3)	84.13(3)	83.55(4)

Table S5 Selected structural parameters (Å, °) for $[Fe(L^2)_2][BF_4]_2\cdot 4CH_3CN$ and $[Fe(L^2)_2][ClO_4]_2\cdot(CH_3)_2CO$, used to monitor their spin states at different temperatures. The bond length data are plotted in Fig. S2.

T (K)	100	150	200	250
$[Fe(L^2)_2][BF_4]_2\cdot 4CH_3CN$				
Average Fe–N{pyridine}[a]	1.910(2)	1.963(3)	2.069(3)	2.107(3)
Average Fe–N{pyrazole}[b]	2.007(3)	2.048(4)	2.135(4)	2.169(4)
Average L^2 bite angle[c]	79.70(14)	78.17(18)	75.18(14)	74.27(17)
$[Fe(L^2)_2][ClO_4]_2\cdot(CH_3)_2CO$				
Average Fe–N{pyridine}[a]	1.903(3)	1.939(4)	2.087(4)	2.115(4)
Average Fe–N{pyrazole}[b]	2.001(4)	2.027(6)	2.154(6)	2.179(6)
Average L^2 bite angle[c]	79.86(19)	78.9(2)	74.5(2)	73.8(3)

[a]Average Fe–N{pyridine} = ½[{Fe(1)–N(2)} + {Fe(1)–N(20)}]
[b]Average Fe–N{pyrazole} = ¼[{Fe(1)–N(9)} + {Fe(1)–N(15)} + {Fe(1)–N(27)} + {Fe(1)–N(33)}]
[c]Average bite angle = ¼[{N(2)–Fe(1)–N(9)} + {N(2)–Fe(1)–N(15)} + {N(20)–Fe(1)–N(27)} + {N(20)–Fe(1)–N(33)}]

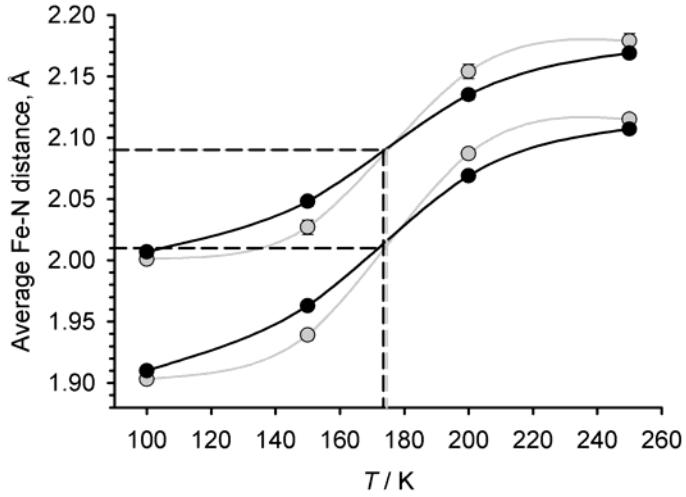

Fig. S2 Plot of the variation of the Fe–N bond lengths with temperature in $[Fe(L^2)_2][BF_4]_2 \cdot 4CH_3CN$ (black) and $[Fe(L^2)_2][ClO_4]_2 \cdot (CH_3)_2CO$ (grey). Data are taken from Table S5, and the averaged Fe–N{pyrazole} and Fe–N{pyridine} distances are plotted separately. The estimated midpoints of the spin-transitions correspond to the temperature at which the average Fe–N distances lie mid-way between the values for the fully high-spin and fully low-spin

Table S6 C–H...I hydrogen bond distances and angles (Å, °) in $[Fe(L^1)_2]I_{0.5}[I_3]_{1.5}$ (**1**).

	C–H	H...I	C...I	C–H...I
C(4)–H(4)...I(39A^{i})	0.95	3.04	3.932(10)	157.1
C(4)–H(4)...I(39B^{i})	0.95	3.00	3.88(2)	154.0
C(4)–H(4)...I(41B^{ii})	0.95	2.96	3.830(19)	153.7
C(6)–H(6)...I(34^{iii})	0.95	3.05	3.999(5)	174.6
C(10)–H(10)...I(35^{iv})	0.95	3.11	4.022(6)	161.9
C(11)–H(11)...I(37^{i})	0.95	3.26	3.933(6)	129.7
C(15)–H(15)...I(39A^{v})	0.95	3.15	4.100(11)	175.1
C(15)–H(15)...I(39B^{v})	0.95	3.12	4.06(2)	171.7
C(15)–H(15)...I(41B^{vi})	0.95	3.25	4.19(2)	169.9
C(16)–H(16)...I(40A^{vii})	0.95	3.13	4.038(8)	160.2
C(16)–H(16)...I(40B^{vii})	0.95	3.18	4.10(2)	161.9
C(17)–H(17)...I(34^{iii})	0.95	3.10	4.033(6)	168.0
C(20)–H(20)...I(37^{v})	0.95	3.08	4.013(5)	166.1
C(21)–H(21)...I(38^{v})	0.95	3.23	3.905(6)	129.4
C(26)–H(26)...I(34)	0.95	3.10	3.926(6)	145.9
C(28)–H(28)...I(37^{v})	0.95	3.23	4.150(6)	162.6
C(31)–H(31)...I(35^{i})	0.95	3.06	3.968(6)	160.3

Symmetry codes: (i) 1–*x*, 2–*y*, 1-*z*; (ii) 1+*x*, 2–*y*, ½+*z*; (iii) 2–*x*, 2–*y*, 1-*z*; (iv) 1–*x*, *y*, ³/₂–*z*; (v) 1–*x*, 1–*y*, 1-*z*; (vi) 1+*x*, 1–*y*, ½+*z*; (vii) 1+*x*, *y*, *z*.